Journal of Nanobiotechnology

RESEARCH

Open Access

A carbon dot nanozyme hydrogel enhances pulp regeneration activity by regulating oxidative stress in dental pulpitis

Yingjuan Zhang[1†], Xianxian Huang[1†], Yicai Luo[1], Xiangyu Ma[1], Ling Luo[1], Ling Liang[2], Tingting Deng[1], Yang Qiao[1], Fanggui Ye[2*] and Hongbing Liao[1*]

Abstract

Preserving pulp viability and promoting pulp regeneration in pulpitis have attracted widespread attention. Restricted by the oxidative stress microenvironment of dental pulpitis, excessive reactive oxygen and nitrogen species (RONS) trigger uncontrolled inflammation and exacerbate pulp tissue destruction. However, modulating redox homeostasis in inflamed pulp tissue to promote pulp regeneration remains a great challenge. Herein, this work proposes an effective antioxidative system (C-NZ/GelMA) consisting of carbon dot nanozymes (C-NZ) with gelatin methacryloyl (GelMA) to modulate the pulpitis microenvironment for dental pulp regeneration by utilizing the antioxidant properties of C-NZ and the mechanical support of an injectable GelMA hydrogel. This system effectively scavenges RONS to normalize intracellular redox homeostasis, relieving oxidative stress damage. Impressively, it can dramatically enhance the polarization of regenerative M2 macrophages. This study revealed that the C-NZ/GelMA hydrogel promoted pulp regeneration and dentin repair through its outstanding antioxidant, antiapoptotic, and anti-inflammatory effects, suggesting that the C-NZ/GelMA hydrogel is highly valuable for pulpitis treatment.

Keywords Nanozyme, Carbon dot, Oxidative stress, Dental pulpitis, Pulp regeneration

Introduction

Pulpitis is inflammation of the dental pulp due to injury or infection. It is one of the widely prevalent oral disorders. Root canal therapy is a successful and established treatment for pulpitis, yet it is a complex, expensive and destructive technique. Although the hard tissues of the tooth are preserved, the inherent biological properties of the pulp, including defensive, developmental and mechanoreceptor features, are eliminated [1]. Contrary to traditional root canal therapy or apexification, vital pulp therapy (VPT), which focuses on the preservation of healthy pulp tissue and minimal intervention, has emerged as a leading treatment recommendation proposed by international endodontic organizations [1, 2]. VPT methods usually comprise direct or indirect

†Yingjuan Zhang and Xianxian Huang contributed equally to this work.

*Correspondence:
Fanggui Ye
fangguiye@163.com
Hongbing Liao
hongbing_liao@gxmu.edu.cn
[1]Guangxi Key Laboratory of Oral and Maxillofacial Rehabilitation and Reconstruction, College & Hospital of Stomatology, Guangxi Medical University, No.10 Shuangyong Road Nanning, Guangxi 530021, China
[2]State Key Laboratory for the Chemistry and Molecular Engineering of Medicinal Resources, School of Chemistry, Pharmaceutical Science of Guangxi Normal University, Guilin 541004, PR China

pulp capping and full or partial pulpotomy. Calcium silicate cements (CSCs) such as mineral trioxide aggregate (MTA), Biodentine, iRoot BP Plus, etc., are currently recommended for VPT [3]. However, it has been shown that both MTA and Biodentine cause an increase in intracellular reactive oxygen species (ROS) levels, which can adversely affect cell viability [4]. Meanwhile, the non-degradable characteristics of CSCs hinder further pulp regeneration, especially in pulpotomy procedures. The flaws in immunomodulation and balancing of the redox environment also compromise the clinical outcome of pulp-capping materials to date [4–6]. Therefore, the development of next-generation of capping biomaterials is urgently needed.

The therapeutic efficacy of VPT is greatly restricted by the endodontic microenvironment, where inflammation accelerates with oxidative stress, ultimately resulting in treatment failure [7, 8]. Excessive reactive oxygen and nitrogen species (RONS) in the inflammatory milieu can cause DNA damage and lipid peroxidation, resulting in loss of cellular function, inhibition of proliferation and induction of apoptosis [9]. Moreover, macrophages, as innate immune effector cells in the dental pulp, can be differentiated into inflammation or healing phases under specific circumstances [10]. Increased RONS production and concomitant oxidative stress in macrophages can serve as a secondary inflammatory response, triggering downstream inflammatory signals, which in turn affect macrophage polarization status and secretion profiles, ultimately impacting tissue repair and regeneration [11]. Therefore, the design of a reliable antioxidant system to modulate oxidative stress for treating dental pulpitis is considered a promising strategy for pulp repair and regeneration.

Substances capable of modulating the oxidative stress environment of the dental pulp include antioxidants [12–14], pharmacological inhibitors [15–17] and bioactive materials [18, 19]. However, the stability, accessibility and therapeutic efficacy of these substances are still lacking, and more effective antioxidant systems remain to be explored and researched. Nanozymes are a type of nanomaterial that can catalyze enzymatic substrates under mild or extreme conditions and have the advantages of high catalytic activity, low cost, and good stability [20]. Nanozymes, with their excellent catalytic properties and selectivity, have made impressive progress in biomedical applications [21]. In particular, nanomaterials with glutathione peroxidase (GPx)-, catalase (CAT)-, and superoxide dismutase (SOD)-like activities have been used as antioxidant nanozymes by modulating the redox environment for various types of antioxidant therapies, such as neurological disease and neurotrauma [22], diabetic wound healing [23], osteoarthritis [24], colitis [25], and periodontitis [26]. Recently, the potential of nanozymes in the treatment of pulpitis has attracted increased amounts of attention [27]. However, the in vivo toxicity of metals and metal oxide nanozymes, i.e., their cytotoxicity and heavy metal accumulation during treatment, are problematic for clinical applications [21]. Moreover, the ability of nanozymes to protect dental pulp stem cells and modulate macrophage polarity in dental pulpitis remains to be explored. Carbon dot nanozymes (C-NZ) with ultrafast electron transfer and superlative catalytic activity, featuring a nitrogen-doped graphene-like core structure, have been shown to have excellent RONS scavenging ability and good biocompatibility [28]. These properties give it great potential for use in the treatment of dental pulpitis. However, the application of nanozymes for pulp regeneration in pulpitis has rarely been reported, possibly due to the lack of ability to act as a tissue engineering scaffold to support pulp regeneration.

Fortunately, bioactive scaffolds can be used as carriers of nanozymes to fulfil the requirement of guided pulp tissue regeneration through stem cell homing [29]. Among these materials, gelatin methacryloyl (GelMA), which can satisfy the requirements of pulp-capping materials, has the advantages of suitable biological properties, adjustable physical properties, and photocrosslinking ability and injectability as a tissue engineering platform for loading C-NZ [30, 31]. Therefore, in this work, we innovatively integrated C-NZ with GelMA to form an antioxidant system (C-NZ/GelMA) and assessed the effectiveness of the C-NZ/GelMA hydrogel in treating dental pulpitis treatment both in vitro and in vivo (Scheme 1). At the cellular level, we found that the C-NZ/GelMA hydrogel effectively scavenged excessive intracellular RONS in the inflammatory microenvironment, reduced oxidative stress-induced cell injury, and greatly facilitated macrophage polarization toward regenerating M2 macrophages. To further evaluate the feasibility of using the C-NZ/GelMA hydrogels as pulp-capping materials, we explored their physicochemical properties and biocompatibility both in vitro and in vivo. The results indicated that the C-NZ/GelMA hydrogel had suitable mechanical properties, an appropriate degradation rate, and a sustainable release ability of the loaded nanoparticles, exhibited excellent biocompatibility, and was capable of facilitating pulp regeneration and dentin repair due to its ability to protect dental pulp cells and promote macrophage polarization to the M2 type. Therefore, the excellent performance of the C-NZ/GelMA hydrogel to protect pulp tissue and modulate the immune response to pulpitis makes it a potentially effective bioactive material for the treatment of pulpitis.

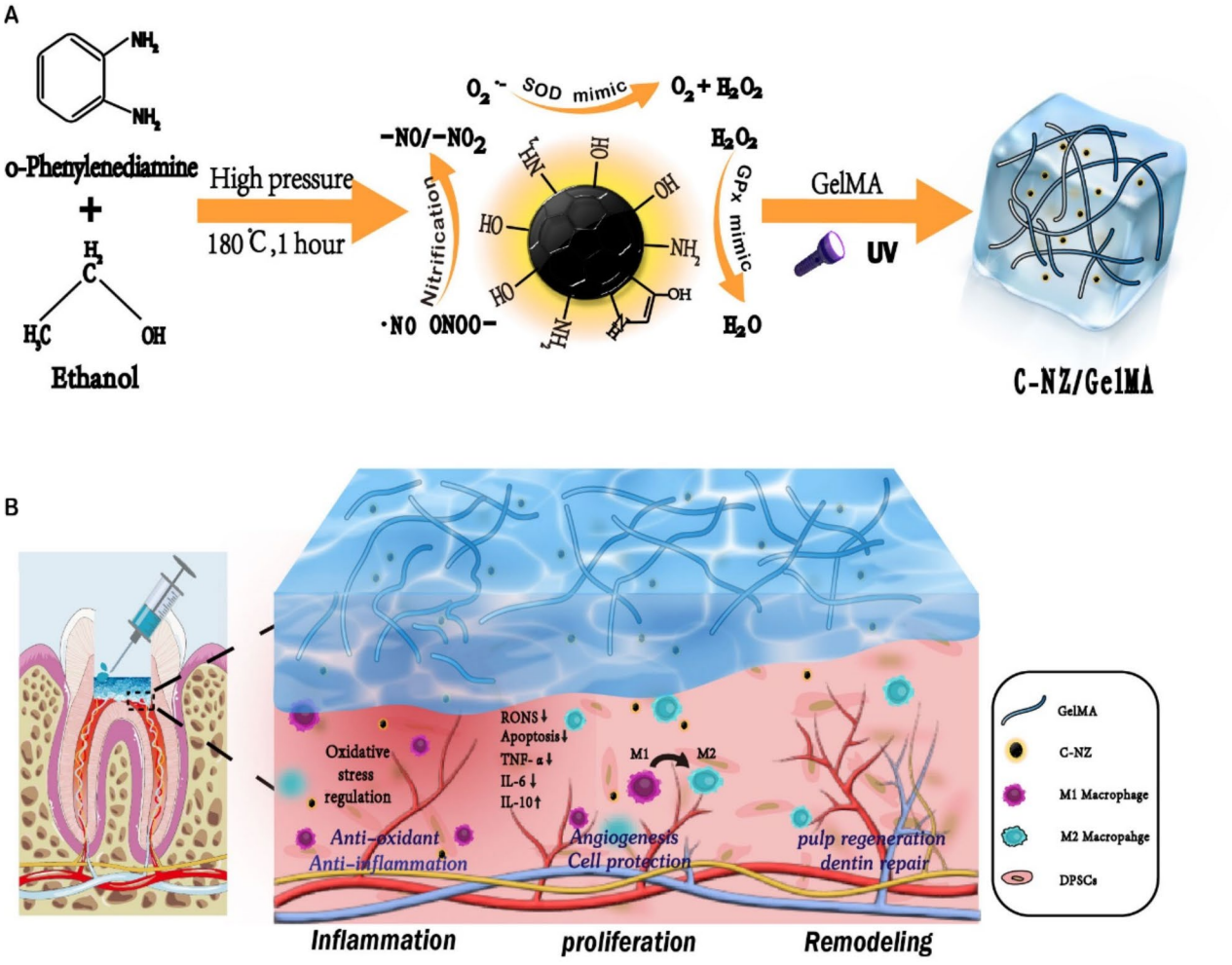

Scheme 1 Schematic illustration of the synthetic procedure of C-NZ/GelMA hydrogel and application for pulpitis treatment. **(A)** The fabrication of C-NZ/GelMA hydrogel. **(B)** The proposed therapeutic mechanisms of C-NZ/GelMA hydrogel

Materials and methods

Materials

Ethanol, 1,1-diphenyl-2-picrylhydrazyl (DPPH), and o-phenylenediamine were acquired from Aladdin (Shanghai, China). GelMA, collagenase II, lithium phenyl (2,4,6-trimethylbenzoyl) phosphinate (LAP), and curing ring were purchased from EFL (Suzhou, China). Gibco (Suzhou, China) supplied 1% penicillin-streptomycin solution, DMEM, and fetal bovine serum (FBS).

Synthesis and characteristic of C-NZ

The synthesis of C-NZ was modified from a previously reported method [28]. Dissolve 1 g of o-phenylenediamine in 100 ml of ethanol in a reaction kettle at 180 °C for 1 h. Remove the ethanol through rotary evaporation and resuspend it in 50 ml of water. The solution is centrifuged through a 3 KD ultrafiltration tube to extract the lower filtrates, and then dialyzed using a 100–500 D dialysis bag for 1 h. The concentration of C-NZ was determined by gravimetry and UV absorption spectroscopy.

High-resolution transmission electron microscopy (HRTEM) images of C-NZ were taken with a Tecnai G2 F20 field emission electron microscope equipped with an energy-dispersive X-ray spectroscopy (EDS) detector (FEI, Japan). The Fourier transform infrared (FTIR) spectrum was carried out using a Nicolet iS50 (Thermo, USA). X-ray photoelectron spectroscopy (XPS) was carried out using an ESCALAB 250Xi X-ray photoelectron spectrometer (Thermo, USA). Absorption spectra were detected via a UV-vis spectrophotometer (Shimadzu, Japan). Emission spectra were obtained using a FluoroMax fluorescence spectrophotometer (HORIBA Scientific, Japan).

Enzyme-mimicking activity of C-NZ

The SOD-mimicking activity of C-NZ was determined using a Total Superoxide Dismutase Kit (Beyotime, China). To begin the reaction, add 20 μl of C-NZ, 160 μl of the WST-8/enzyme working solution, and 20 μl of the reaction initiator were added sequentially. The absorbance was measured at 450 nm after the reactions were incubated for 30 min at 37 °C.

The GPx-mimicking activity of C-NZ was tested utilizing a Total Glutathione Peroxidase Assay Kit (Beyotime, China). The assay system consisted of 50 μl of C-NZ solution at different concentrations, 40 μl of GPx assay working solution, and 10 μl of peroxide solution. The enzyme activity data for GPx were obtained by continuously measuring the A340 at 25 °C for 5 min using a microplate reader.

Synthesis of the C-NZ/GelMA hydrogel

The GelMA (60% amino substitution) was added to a 0.25% (w/v) LAP solution, and the mixture was heated in a water bath at 60–70 °C in the dark for 20–30 min. Then, the appropriate amount of C-NZ solution (100 μM, the storage concentration) was mixed and stored it in a light-protected environment. The proportions of all hydrogel components are shown in Table S1.

Material properties of the C-NZ/GelMA hydrogel

Scanning electron microscopy (SEM) images of the hydrogels were characterized by a Sigma300 (ZEISS, Germany). To assess the photocurable characteristics of the C-NZ/GelMA hydrogels, an in-situ photo-rheology analysis was conducted using a rotational speed of 5 rad/s and a 1% strain. G' and G" were determined at a frequency of 1 Hz. The hydrogels were cast into a circular mold with a diameter of 20 mm and a height of 5 mm, and compression tests were then conducted at a rate of 1 mm/min and 25 °C using an electronic universal testing machine (Instron-9569, USA).

400 μl of the C-NZ/GelMA hydrogel was made into a 0.5 cm diameter disc and submerged in 2 ml of PBS at 37 ℃ to observe the swelling properties. Subsequently, the PBS was removed at 0, 2, 6, 12, 24, and 36 h, and the samples were weighed to determine the swollen weight (Ws). The ultimate dry mass (Wd) of samples was determined after 24 h of freeze-drying. The swelling ratio was defined by the following formula [32]:

$$Swelling\ ratio = \frac{W_s - W_d}{W_d} \times\ 100\%$$

To observe the sustained release properties, 1 ml the C-NZ/GelMA hydrogel was made into a disk 1 cm in diameter and immersed in 5 ml PBS (pH=7.2–7.4) placed in a shaker (37 °C, 100 rpm). 500 μl of supernatant was collected for analysis at the predefined time points and supplemented with an equal amount of fresh PBS. The C-NZ concentration of the supernatant was determined from the UV-concentration standard curve.

A disk with a diameter of 0.5 cm was prepared from 200 μl of C-NZ/GelMA for in vitro degradation experiments. The materials were submerged in 5 ml of PBS containing 2 U of collagenase II, collected at 0, 2, 4, 6, and 8 h and then freeze-dried. The weight of the samples after freeze-drying corresponds to Wd (0 h corresponds to W_{d0}, and the sequence time point sample weight corresponds to W_{dn}). The following equation was used to calculate the mass degradation ratio (DR in vitro):

$$DR_{in\ vitro} = \frac{W_{d0} - W_{dn}}{W_{d0}} \times\ 100\%$$

In vitro RONS scavenging activities of C-NZ and C-NZ/GelMA

The ROS scavenging capacity of C-NZ was assessed by a T-AOC Assay Kit (Beyotime, China). 200 μl of 2,2′-azinobis (3-ethylbenzthiazoline-6-sulfonic acid (ABTS) working solution and 10 μl of varying concentrations of C-NZ solution were gently agitated. The absorbance at 405 nm was measured with a microplate reader. PBS was added as a blank control. ROS scavenging efficiency of C-NZ under different pH conditions was calculated using the following formula:

$$Scavenge\ efficiency\% = \frac{A_{blank} - A_{sample}}{A_{blank}} \times\ 100\%$$

To assess the antioxidant ability of C-NZ against reactive nitrogen species (RNS), 200 μl of DPPH/ethanol (40 μg/ml) and 10 μl of C-NZ solution were added in each well of a 96-well plate, and the absorbance at 517 nm was measured with a microplate reader.

To assess the antioxidant capacity of the hydrogels, 100 μl of the hydrogel was spread at the bottom of a 96-well plate. Subsequently, the assay reagents were added according to the two methods mentioned above. After thorough mixing, 200 μl of the supernatant was collected for absorbance measurement using a microplate reader.

Cell culture and identification

The research received ethical approval from the Ethics Committee of Guangxi Medical University (Protocol Number: 2023015) and informed consent was obtained from the patients. Human dental pulp stem cells (hDPSCs) were extracted from healthy human dental pulp tissue utilizing a methodology previously described in the literature [33]. Cells from the third to fifth passages

were employed in subsequent experimental procedures. RAW264.7 cells were purchased from American Type Culture Collection (ATCC). The hDPSCs and RAW 264.7 cells were cultured in an incubator containing 5% CO_2 at 37 °C with Dulbecco's modified Eagle's medium (DMEM) containing 10% FBS and 1% penicillin-streptomycin.

hDPSCs were characterized by their multipotent differentiation capacity and surface markers. Osteogenesis, adipogenesis, and chondrogenesis differentiation of hDPSCs were induced using the Osteogenic Differentiation, Adipogenic Differentiation, and Chondrogenic Differentiation kits (Cytogen, China), and then observed by corresponding staining using Alizarin Red, Oil Red O and Alcian Blue. The surface molecular markers CD90, CD29, CD34, and CD45 (BD Pharmingen, USA) were evaluated on hDPSCs using flow cytometry (FCM).

Cellular uptake

To observe the cellular uptake, RAW264.7 cells or hDPSCs were incubated with culture medium containing C-NZ (10 μM) for 24 h. Then, the cells were fixed with 4% paraformaldehyde and then stained with DAPI (Abcam, USA). Fluorescence microscopy (Olympus, Japan) was used to investigate cellular internalization.

Preparation of hydrogel extracts and cellular biocompatibility

The GelMA and C-NZ/GelMA with different C-NZ concentrations (1 ml volume) were submerged in 5 ml of complete medium at 37 °C for 24 h to obtain the hydrogel extracts.

For the cytotoxicity evaluation, hDPSCs (1×10^4 cells/well) were seeded in 96-well plates and incubated with the extract medium for 24 h. Cell viability was determined by the CCK-8 assay (Beyotime, China).

To observe the adhesion behavior and survival of hDPSCs in the surface of hydrogels, 180 μl of hydrogel was dropped into a curing ring and exposed to UV light for 30 s at 405 nm for solidification. After that, the ring was placed in a 24-well plate, and hDPSCs were seeded onto the surface at 3×10^4 cells/well and cultured conventionally for 24 h. When 3D cell culture was performed, 10 μl of hDPSCs cell suspension containing 4×10^5 cells was homogeneously mixed with 180 μl of uncured hydrogels. Then, the hydrogel mixed with cells was dropped into curing ring cured and placed in a 24-well plate for culture. Cell adhesion was assessed using phalloidin/4,6-diamino-2-phenylindole staining (Beyotime, China). Cell survival was assessed using Live/Dead Staining Kit (Beyotime, China). The results were observed by a confocal microscope (Zeiss, Germany).

Cell treatment categorization

The cells were divided into 4 groups: (1) Control group: cells were cultured normally without any treatment; (2) LPS group: cells were incubated with *Porphyromonas gingivalis* lipopolysaccharide (*Pg*-LPS) (InvivoGen, USA); (3) LPS+GelMA group: *Pg*-LPS induced cells were treated with GelMA extract medium; (4) LPS+C-NZ/GelMA group: *Pg*-LPS induced cells were treated with C-NZ/GelMA extract medium.

Intracellular RONS measurement

An oxidative stress environment was created using *Pg*-LPS (10 μg/ml), and different hydrogel extracts were used to treat the cells. Detection was verified using Reactive Oxygen Species Assay Kit for general ROS and Nitric Oxide Fluorescent Probe Detection Kit for NO levels (Beyotime, China), respectively. Intracellular oxidative stress was visualized through a fluorescence microscope, and free radicals were quantified using FCM.

Antioxidant properties of hydrogels

To test the cell survival rate, hDPSCs (1×10^4 cells/well) were incubated with *Pg*-LPS (10 μg/ml) or H_2O_2 (200 μM) (Sigma Aldrich, USA) for 6 h. The culture media was then replaced with hydrogel extracts, and cell viability was assessed using the CCK-8 test after a further 24 h of incubation.

The Live/Dead Staining Kit (Beyotime, China) was used to assess cell viability. The hDPSCs were treated with *Pg*-LPS (20 μg/ml) according to the above procedure, and then stained with calcein-AM (1 μM) and propidium iodide (PI, 1 μM). The dead and live cells were recorded with a fluorescence microscope (Olympus, Japan).

Annexin V-APC/7-AAD Apoptosis Detection Kit (eBioscience, USA) was utilized to detect and analyze cell apoptosis in each group by FCM cytometer (FACSCanto, BD).

In vitro macrophage polarization

RAW264.7 cells (4×10^5 cells/well) were seeded in a 6-well plate and cultured with the extract medium or complete culture medium containing *Pg*-LPS (10 μg/ml) for 24 h. The trend of RAW264.7 cells polarization was assessed through FCM, qPCR, and ELISA.

RAW264.7 cells subjected to different treatments were collected and stained with anti-CD86-APC and anti-CD206-PE antibodies (eBioscience, USA), followed by FCM analysis.

qPCR was used to analyze the expression levels of inflammatory genes (iNOS and ARG1). Total RNA was extracted with TRIZOL and cDNA was reverse transcribed with PrimeScript (Takara, Japan). For qPCR, SYBR premix was added to cDNA in a real time PCR system (GenStar, China), preincubated with 1 cycle at

95 ℃ for 2 min, and then amplified with 40 cycles at 95 ℃ for 15 s and 60 ℃ for 30 s. Relative mRNA expression was quantified by the 2-ΔΔCt method and normalized to GAPDH. The experiment was repeated in triplicate. The primer sequences used in the qPCR experiments are shown in Table S2.

Supernatants from various treatment groups were analyzed using ELISA. The Mouse TNF-α ELISA Kit and Mouse IL-10 ELISA Kit (FANKEW, China) were used to quantify the amount of TNF-α and IL-10 as per the manufacturer's instructions.

Animal experiments

All the animals were procured from the Experimental Animal Center of Guangxi Medical University. All experimental procedures were conducted in compliance with the guidelines set by the Animal Research Ethics Committee of Guangxi Medical University (Protocol Number: 202307435,202307004).

Pulp capping treatment in the rat dental pulpitis model

A total of 30 male Sprague-Dawley (SD) rats, weighing between 200 and 250 g, were used for this experiment. The rats were divided into four groups based on the treatment protocol: Control group (untreated); Pulpitis group; Pulpitis + GelMA group; Pulpitis + C-NZ/GelMA group.

Dental pulpitis models were established in the upper incisors and the maxillary first molars of rats. Rats were anesthetized with 2% pentobarbital sodium (2 ml/kg) by intraperitoneal injection. The pulp chambers were exposed using a round bur (0.5 mm diameter). For the incisors, the upper segment of the root canal was cleaned with a $40^{\#}$ K file, it was sealed with *Pg*-LPS (1 mg/ml) paper points for 2 days. For the maxillary first molars, the mesial pulp chamber was enlarged to the size of $60^{\#}$ K file, some coronal pulp was removed, and *Pg*-LPS (1 mg/ml) paper points were sealed for 30 min. Subsequently, the paper points were removed, and the pulp chambers were rinsed with physiological saline. GelMA was injected into the pulp chamber of the left-side treated teeth, while C-NZ/GelMA was injected into the right-side treated teeth. UV light curing was performed for 40 s, and the surface of the hydrogel was covered with iRoot BP Plus, followed by light-curing resin filling.

Pulpitis + GelMA group and Pulpitis + C-NZ/GelMA group experimental teeth were collected on day 3 and day 7. In addition to this, maxillary first molars were collected on day 35 to assess pulp regeneration and reparative dentin formation. The Pulpitis group was sacrificed immediately after the completion of the dental pulpitis model was established. Teeth were extracted from each group for further H&E, Mason, TUNEL, CD86 and CD206 immunofluorescence staining, and micro-CT evaluation.

Levels of oxidative stress and inflammation

The dental pulp tissues from each group's upper incisors were isolated and preserved in liquid nitrogen. Hydrogen peroxide levels were determined using a Hydrogen Peroxide Assay Kit (Beyotime, China), and the NO content was measured using a Total Nitric Oxide Assay Kit (Beyotime, China). SOD activity was assessed using the Total Superoxide Dismutase Assay Kit with WST-8 (Beyotime, China). GPx activity was assessed using the Total Glutathione Peroxidase Assay Kit with nicotinamide adenine dinucleotide phosphate (NADPH) (Beyotime, China). ELISA kits (Fankew, China) were used to measure the levels of TNF-α, IL-6, and IL-10 in the dental pulp tissues.

Subcutaneous transplantation experiment

A total of six male Kunming mice, weighing approximately 50 g, were employed for this experiment. The mice were anesthetized with an intraperitoneal dose of pentobarbital. 200 μl of the C-NZ/GelMA hydrogel was prepared into a circular disc with a diameter of 0.5 cm and subcutaneously transplanted into the dorsal area of the mice. Using an animal live imaging system (AniView, China), the degradation of the gel and the release of C-NZ were observed at predetermined time points (0, 6, 14, 21, 28, and 35 days). The mice were sacrificed on day 35. The residual hydrogel along with surrounding soft tissues, as well as the heart, liver, spleen, lungs, and kidneys, were stained with H&E.

Statistical analysis

GraphPad Prism software (version 8.4.3) was used to generate all statistical analyses. All data are presented as mean ± SD, $n=3$. For normally distributed data sets with equal variances, one-way ANOVA testing followed by a Tukey multiple comparisons test was carried out across groups, and *p value less than 0.05 was considered statistically significant. No significant difference are presented as ns, and statistical significance are presented as $^{*}P<0.05$; $^{**}P<0.01$; $^{***}P<0.001$ and $^{****}P<0.0001$.

Results and discussion

Characterization of C-NZ

Typical HRTEM images revealed that the C-NZ nanoparticles had a monodisperse spherical shape with an average diameter of approximately 3.2 nm (Fig. 1A and B). Furthermore, the EDS elemental mapping data showed a homogeneous distribution of 95.27% C, 0.7% N, and 4.03% O (Fig. 1C and Figure S1). Without additional alteration, C-NZ in an aqueous solution has good dispersity and a brownish yellow hue. Under excitation by 365 nm ultraviolet light, C-NZ exhibits bright yellow fluorescence emission (Figure S2). The UV-vis absorption spectra of C-NZ reveal a unique peak at ~432 nm

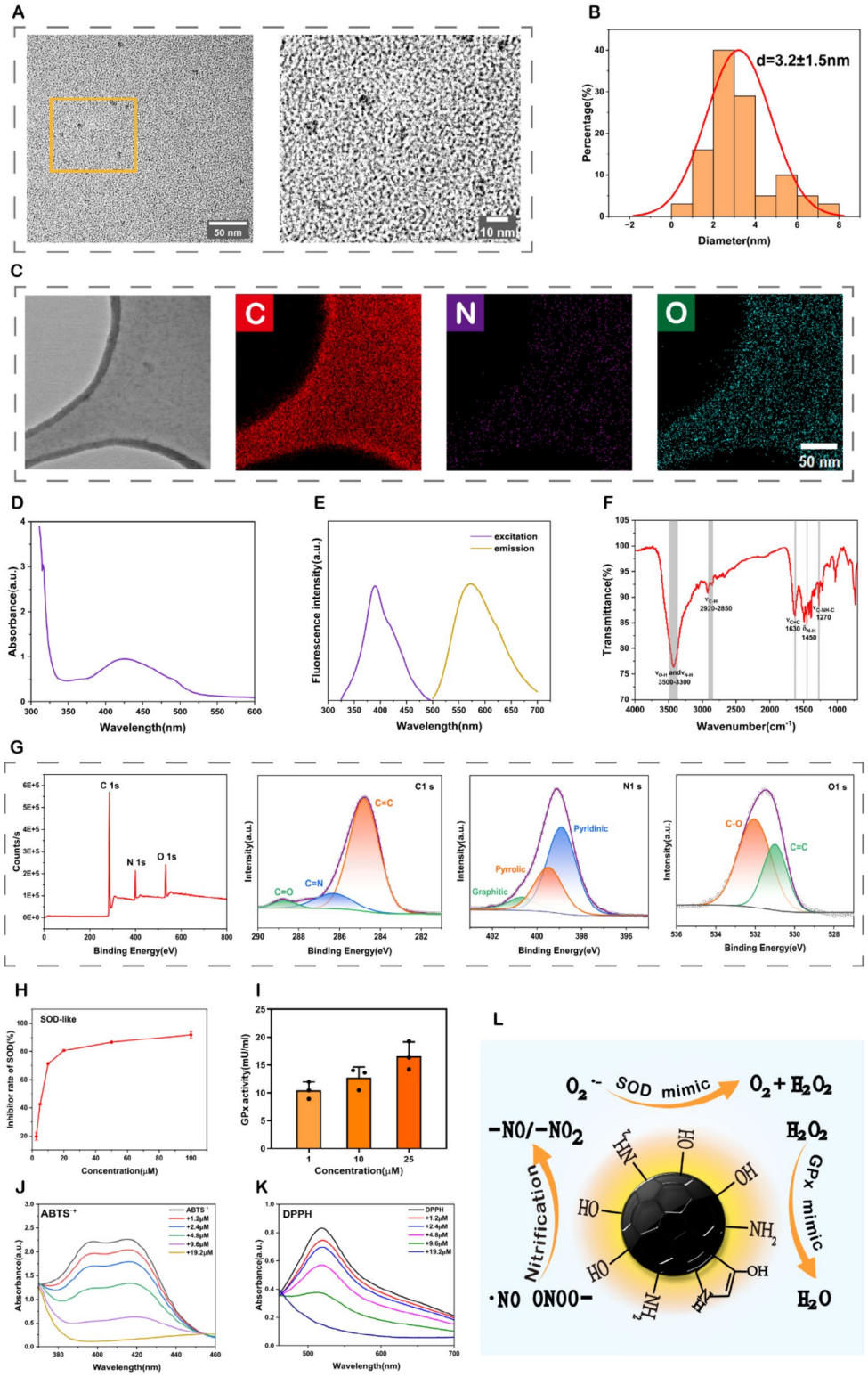

Fig. 1 Characterization of C-NZ. **(A)** The image of HR-TEM. Scale bars indicate 50 μm (left figure) and 10 μm (right figure), respectively. **(B)** Size distribution of C-NZ. **(C)** EDS elemental mapping images of C-NZ. **(D)** UV–vis absorption spectrum. **(E)** Excitation and emission photoluminescence spectrum. **(F)** FTIR spectrum. **(G)** XPS spectrum. **(H)** Inhibitor rate of SOD-like activity for C-NZ. **(I)** GPx-like activity of C-NZ. **(J)** Absorption spectra of $ABTS^{\cdot+}$ aqueous solution added with different concentration C-NZ. **(K)** absorption spectra of DPPH solution added with different concentration C-NZ. **(L)** Schematic diagram of SOD- and GPx- like activities and RONS scavenging routes of C-NZ. Data are expressed as mean ± SD ($n = 3$)

(Fig. 1D). The fluorescence spectra show an emission peak at 573 nm with an excitation wavelength of 390 nm (Fig. 1E). The above structures and properties confirm that C-NZ conforms to the characteristics of carbon dots [34].

The surface chemical features were studied using FTIR and XPS. The peaks at 3500−3300 and 2920−2850 cm^{-1} correspond to N–H/O–H and C–H stretching vibrations, respectively. The peaks at 1270, 1450 and 1630 cm^{-1} represent C–NH–C stretching bands, amide N–H bending and C=C stretching, respectively (Fig. 1F). The FITC results indicated the presence of hydroxyl and amino groups in C-NZ, and the presence of a large number of hydroxyl groups on the surface of carbon cores enhanced the hydrophilicity of C-NZ nanoparticles [35]. XPS reveals that C-NZ is predominantly composed of C, N, and O components. Furthermore, the deconvolution of C1s spectra yields three peaks at 284.78, 286.28 and 288.68 eV, which correspond to the C=C, C=N, and C=O groups, respectively. Similarly, the N1s peak can be separated into the distinctive peaks of pyridinic N, pyrrolic N and graphitic N (398.68, 399.38 and 400.18 eV), whereas the O1s peaks can be dissected into C=O and C–O bonds (530.98, and 532.08 eV) (Fig. 1G). As a result, C-NZ possesses a nitrogen-doping graphitic structure as its core and amide, hydroxyl, and pyrrolic groups as surface functional groups, as previously reported [28]. The presence of these electron donors and acceptors can enhance the intramolecular charge transfer effect, which promotes catalytic activity.

SOD is an important antioxidant enzyme that catalyzes the disproportionation of $O_2^{\bullet-}$ to convert H_2O_2 and O_2. As shown in Fig. 1H, with increasing C-NZ concentration, the ability to scavenge $O_2^{\bullet-}$ free radicals increased, and 20 μM C-NZ eliminated approximately 80% of $O_2^{\bullet-}$, demonstrating the ability of C-NZ to mimic the natural SOD enzyme. GPx can utilize reduced glutathione (GSH) to catalyze the decomposition of H_2O_2 to H_2O, thus completing the cascade reaction of ROS scavenging. In this study, an indirect assay was utilized to calculate the GPx-like activity of C-NZ by detecting the reduction of NADPH. C-NZ nanoparticles exhibited dose-dependent GPx-like activity, reaching 17 mU/ml at 25 μM (Fig. 1I).

The ability of the C-NZ nanozymes to scavenge RONS was evaluated via ABTS and DPPH scavenging experiments. The reduced absorbance equals to higher antioxidant property in ABTS and DPPH assay. Trolox has antioxidant capacity similar to that of vitamin E. The ABTS assay revealed that the total antioxidant activity of C-NZ was approximately 25-fold greater than that of Trolox, indicating that C-NZ had high scavenging activity against ROS (Figure S3A). Furthermore, the ability of C-NZ to scavenge ROS was concentration dependent (Fig. 1J and Figure S3B). Even at pH 4, C-NZ retained 75% of $ABTS^{\cdot+}$ scavenging efficacy (Figure S3C). DPPH is utilized to assess the activity of antioxidants in scavenging RNS [36]. C-NZ effectively and continuously scavenged DPPH, demonstrating its strong scavenging ability to scavenge RNS in a dose-dependent manner (Fig. 1K and Figure S3D).

C-NZ has significant RONS scavenging activity and enzyme-like activity, which can be attributed to its graphitic core structure, the synergistic impact of amide, hydroxy, and pyrrolic surface groups acting as hydrogen donors and more active centers [28].Figure L presents the scavenging of RONS by C-NZ nanozymes with SOD- and GPx-like activities through multiple reactions.

Physicochemical characterization of C-NZ/GelMA hydrogel and its excellent biocompatibility

The physicochemical properties of C-NZ/GelMA hydrogels are important for assessing their potential as pulp-capping materials for promoting pulp regeneration. Therefore, formability, injectability, mechanical properties, swelling behavior, sustained release and degradation were carefully investigated.

Cross-linked C-NZ/GelMA hydrogel was yellow jelly-like, which could adapt to complex morphology and had a certain mechanical strength. The microscopic morphology of C-NZ/GelMA hydrogels showed that they had a similar pore size to GelMA, forming a homogeneous porous interconnected network. C-NZ nanoparticles were uniformly dispersed on the surface of C-NZ/GelMA hydrogel pores (Fig. 2A). C-NZ/GelMA hydrogel can rapidly transform from a liquid to a gel upon exposure to blue light (405 nm) for 30 seconds (Fig. 2B). Rheological tests further evaluated the photosensitivity of C-NZ/GelMA hydrogels. Before photo-crosslinking, storage modulus (G') and loss modulus (G") of C-NZ/GelMA hydrogel were approximately 1×10^{-1}, indicating excellent flowability and injectability. After photo-crosslinking, G' rapidly increased to 1×10^{3}, indicating a sol-gel transition of C-NZ/GelMA hydrogel (Fig. 2C). The excellent formability and injectability of the C-NZ/GelMA hydrogel make it particularly adaptable to the complex morphology of the pulp chamber.

The addition of C-NZ did not alter the mechanical properties of GelMA, possibly attributed to the tiny dosage of C-NZ. When the pressure was less than 20Kpa, C-NZ/GelMA hydrogel exhibited no obvious elastic deformation (Fig. 2D). The C-NZ/GelMA hydrogel has a compression modulus of 10 kPa, similar to that of human pulp tissue(5.5±2.8 kPa) [37], which may facilitate the adhesion, proliferation and differentiation of hDPSCs and provide support for the filling of hydrogel surface materials [38].

Furthermore, we investigated the swelling kinetics of C-NZ/GelMA hydrogel. All the hydrogels swelled rapidly

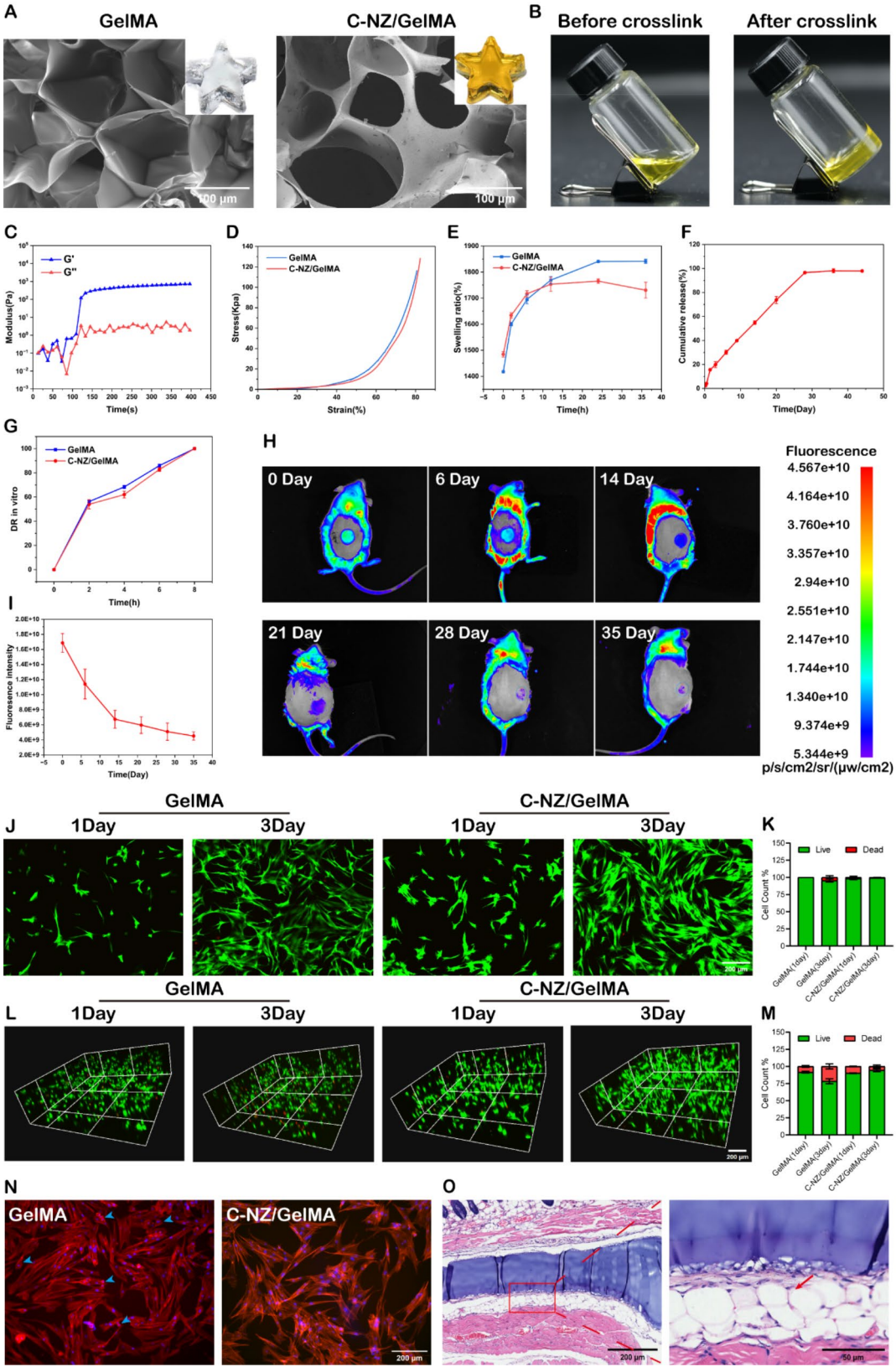

Fig. 2 (See legend on next page.)

(See figure on previous page.)

Fig. 2 Physicochemical characterization of C-NZ/GelMA hydrogel and its excellent biocompatibility. **(A)** SEM images and the macroscopic images of hydrogels. Scale bar = 100 μm. **(B)** Images showing C-NZ/GelMA hydrogel before and after cross-linking. **(C)** Rheological testing of C-NZ/GelMA hydrogel. **(D)** Stress-strain curves of hydrogels. **(E)** The swelling ratio of the hydrogels. **(F)** Cumulative release rate curve of C-NZ from C-NZ/GelMA hydrogel. **(G)** In vitro degradation ratio (DR) of hydrogels. **(H)** The fluorescence signal variation of C-NZ/GelMA in the dorsal region over time. **(I)** Fluorescence decay curves of C-NZ/GelMA hydrogels in subcutaneous tissue. **(J)** Live/Dead staining of hDPSCs in 2D culture and **(K)** quantitative analysis (Green/red represent live/dead cells respectively). Scale bar = 200 μm. **(L)** Live/Dead staining of hDPSCs in 3D culture and **(M)** quantitative analysis (Green/red represent live/dead cells respectively). Scale bar = 200 μm. **(N)** Cytoskeleton and nuclei staining (F-actin/DAPI) for hDPSCs -laden GelMA and C-NZ/GelMA hydrogels. Arrows indicated reduced cell viability and cytoskeletal defects. Scale bar = 200 μm. **(O)** H&E staining of the subcutaneous tissues on day 35. Scale bars indicate 200 μm (left figure) and 50 μm (right figure), respectively. Data are expressed as mean ± SD ($n = 3$)

within 2 h. The GelMA hydrogels had an initial swelling ratio more than 1400% and reached the swelling equilibrium around 24 h, with an increase in swelling ratio of about 393%. The C-NZ/GelMA hydrogel had an initial swelling rate of nearly 1500% and reached the swelling equilibrium around 12 h, with an increase in swelling ratio of about 265% (Fig. 2E). The porous structure and the abundance of hydroxyl groups endow hydrogels with good water storage capacity, which can mimic the natural microenvironment and support normal cellular activities and tissue metabolism [39, 40]. The pulpal cavity is a relatively closed space, and excessive swelling may put additional pressure on the pulp during the inflammatory process, which is not helpful for the recovery of pulpitis. Therefore, a greater initial water content of C-NZ/GelMA hydrogel, faster attainment of swelling equilibrium and a lower final swelling rate may be more suitable as a scaffold for pulp regeneration in pulpitis.

According to the release curve of C-NZ/GelMA hydrogel, approximately 15% of C-NZ was released within 36 h, followed by entering a slow and steady release state, with a release period lasting up to 28 days (Fig. 2F). The sustained release ability may be related to the carboxyl and hydroxyl groups on the surface of C-NZ, which can form hydrogen bonds with the carboxyl and amide groups of the GelMA polymer chains [41]. This aligns with the progression of dental pulpitis, where dental pulp infection gradually transitions into a slow tissue repair process after the initial peak of inflammation.

In vitro degradation, there was no significant difference between the two hydrogels. Approximately 60% of the hydrogels were degraded within 2 h and completely degraded in 8 h (Fig. 2G). This finding is consistent with previous literature reports [42], indicating that C-NZ/GelMA hydrogels rapidly degrade under the action of collagenase II. Considering the more complex in vivo environment, C-NZ/GelMA hydrogels were implanted under the dorsal skin of mice to observe in vivo degradation. The fluorescence properties of carbon dots were employed to monitor the fluorescence signal of C-NZ/GelMA hydrogels in vivo. Figure 2H and I show a progressive decline in the fluorescence signal strength and area of the samples over time, with a relatively rapid degradation in the initial 15 days, reaching near-complete degradation of the hydrogels by day 35. This degradation process was much slower than the in vitro degradation process, suggesting that the degradation of C-NZ/GelMA hydrogels in vivo is not only enzyme-dependent but may also involve a complex immune response.

Biocompatibility is a crucial aspect of biomaterial science. hDPSCs, which serve as the foundation for pulpal tissue repair and regeneration, were extracted and characterized (Figure S4). The cell compatibility of C-NZ/GelMA hydrogels on hDPSCs was evaluated through cytotoxicity tests, live/dead cell staining and cytoskeleton staining. The results of cytotoxicity experiments showed that C-NZ/GelMA hydrogels containing 10–30 μM C-NZ nanoparticles were not cytotoxic (Figure S5). Live/dead cell staining was used to observe the survival and proliferation abilities of hDPSCs. In 2D culture, both groups had good cell adhesion and proliferation with few dead cells (Fig. 2J and K). However, on day 3 of 3D culture, many hDPSCs died in the GelMA group, while few cells died and abundant hDPSCs proliferated in the C-NZ/GelMA group (Fig. 2L and M). This may be related to the fact that C-NZ nanoparticles ameliorated the oxidative stress and hypoxia of the cells during 3D culture. Cytoskeleton staining after 24 h of cultivation revealed that some cells on the surface of the GelMA hydrogel showed altered morphology, such as shrinkage, rounding or abnormal cytoplasmic extension, indicating reduced cell viability and impaired cytoskeletal integrity. hDPSCs were capable of settling on the surfaces of C-NZ/GelMA hydrogels, exhibiting shuttle or triangular shapes and cytoskeletal integrity (Fig. 2N). Overall, C-NZ/GelMA hydrogel favors the adhesion and proliferation of stem cells. Histological analysis revealed that the implanted C-NZ/GelMA hydrogel was surrounded by fibrous connective tissue with a few immune cells (labeled by arrow). Furthermore, no apparent necrosis or inflammation was observed in the surrounding tissues of the graft, implying that the hydrogel was well tolerated by the host animal (Fig. 2O). No abnormalities, such as degeneration, atrophy, or necrosis, were detected in important organs, such as the heart, lungs, liver, kidneys, or spleen (Figure S6). These results demonstrate the high biocompatibility of C-NZ/GelMA hydrogel.

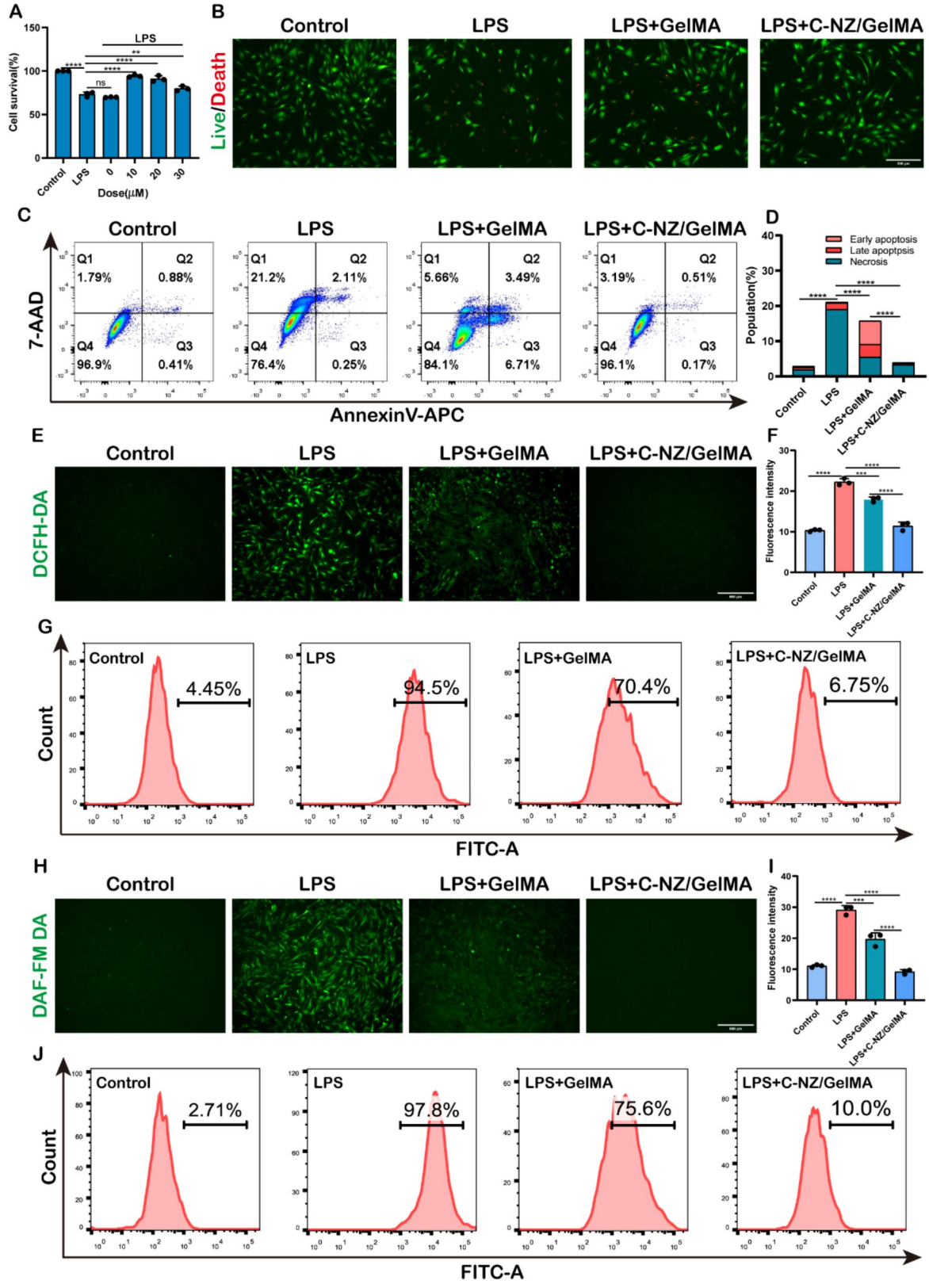

Fig. 3 (See legend on next page.)

(See figure on previous page.)

Fig. 3 The effects of C-NZ/GelMA hydrogel in antioxidation and protection of hDPSCs. **(A)** Evaluation of hDPSCs survival under *Pg*-LPS with treatment of C-NZ/GelMA hydrogels with different C-NZ concentrations by CCK-8 assays. **(B)** Images of hDPSCs after various treatments were stained using calcein/PI immunofluorescence, with calcein (green)/PI (red) stained live/dead cells, respectively. Scale bar = 600 μm. **(C)** Cell apoptosis of *Pg*-LPS induced hDPSCs with different treatments and **(D)** FCM analysis of the related apoptosis cells. **(E)** Fluorescence images of the total ROS observed in *Pg*-LPS treated hDPSCs using DCFH-DA probe and **(F)** quantitative fluorescence intensities **(G)** corresponding the total ROS level by the FCM. Scale bar = 600 μm. **(H)** Fluorescence images of •NO level tested by the fluorescent probe DAF-FM DA and **(I)** quantitative fluorescence intensities **(J)** the corresponding quantitative result using FCM. Scale bar = 600 μm. Data are expressed as mean ± SD, $n = 3$. P-values are calculated using one-way ANOVA with Tukey's multiple comparisons test (ns, not significant; *$P<0.05$; **$P<0.01$; ***$P<0.001$ and ****$P<0.0001$)

Intracellular antioxidative activity and cytoprotective effect of C-NZ/GelMA hydrogels

Elevated levels of local ROS in dental pulpitis contribute to the decline in the quantity and functionality of DPSCs, exacerbating dental pulp tissue damage and hindering tissue repair [43]. As a result, modulating and restoring local ROS levels may increase stem cell survival and functional recovery, thereby boosting dental pulp tissue regeneration. We evaluated the cytoprotective effects of the hydrogel under *Pg*-LPS or H_2O_2-induced oxidative stress conditions in hDPSCs. Co-culturing cells with *Pg*-LPS or H_2O_2 resulted in significant decrease in survival rate. Upon addition of C-NZ/GelMA hydrogel extracts following treatment with *Pg*-LPS or H_2O_2, cell viability was restored (Fig. 3A and Figure S7). Notably, C-NZ/GelMA containing 10 μM C-NZ significantly improved the survival rate of *Pg*-LPS-stimulated hDPSCs from 73 to 94%, while the survival rate of H_2O_2-stimulated cells increased from 71 to 145%, suggesting that C-NZ/GelMA containing 10 μM C-NZ exerted the strongest protective effect on hDPSCs. Consequently, C-NZ/GelMA hydrogel with 10 μM C-NZ was selected for this study.

Subsequent staining of the hDPSCs with the live/dead cell dye solution demonstrated that *Pg*-LPS-induced oxidative stress led to cell death. The C-NZ/GelMA group exhibited a significantly lower percentage of dead cells, indicating that the cells were effectively protected from cell death caused by oxidative stress (Fig. 3B). Consistent results were observed in apoptosis flow cytometry experiments, where C-NZ/GelMA effectively reduced cell necrosis and apoptosis induced by *Pg*-LPS (Fig. 3C and D).

The stable fluorescence characteristics of carbon dots facilitated the observation of the cellular uptake of C-NZ. A large accumulation of green fluorescent C-NZ nanoparticles in the cytoplasm was observed under fluorescence microscopy, thus laying the foundation for effective RONS scavenging (Figure S8). To assess the antioxidant activity of the C-NZ/GelMA hydrogels, we conducted ABTS and DPPH free radical scavenging experiments. The results showed that C-NZ/GelMA hydrogel had remarkable RONS scavenging capabilities (Figure S9). Subsequently, we further evaluated its antioxidant effect on hDPSCs. To assess the total intracellular ROS levels following labeling with the 2′,7′-dichlorofluorescin diacetate (DCFH-DA) probe, we utilized direct observation and FCM analysis (Fig. 3E-G). Figure 3E shows representative fluorescence images of ROS levels in the different group. Following *Pg*-LPS treatment, the intracellular green fluorescence intensity in the LPS group rose considerably compared to that in the control group, indicating an elevation in intracellular ROS intensity. After treatment with C-NZ/GelMA hydrogel extracts, ROS levels were restored to levels close to those in the control group. FCM analysis revealed that ROS levels in hDPSCs reduced dramatically from 94.5% (LPS group) to 6.75% after C-NZ/GelMA treatment, while those in the GelMA group decreased only marginally to 70.4%. 4-Aminomethyl-2′,7′-difluorescein diacetate (DAF-FM DA), a cell-permeable fluorescent marker sensitive to RNS, was used to detect RNS within cells. The same trends were achieved for •NO radical scavenging, demonstrating that C-NZ/GelMA significantly reduced intracellular •NO radical levels induced by *Pg*-LPS, protecting cells from •NO radical damage (Fig. 3H-J).

In summary, the C-NZ/GelMA hydrogel demonstrated excellent biocompatibility in vitro and enhanced hDPSCs proliferation. Moreover, C-NZ/GelMA hydrogels were able to efficiently scavenge intracellular RONS, which had a significant cytoprotective effect and attenuated apoptosis under oxidative stress. The superior antioxidant activity of hydrogels makes them a potential therapeutic strategy for protecting pulp cells and promoting pulp tissue regeneration in oxidative stress environments.

Enhanced M2 polarization of RAW264.7 cells

Numerous studies indicate that stimulation of macrophages with bacterial components increases the production of RONS [44–46]. RONS are inflammatory response products that regulate the production of pro- and anti-inflammatory cytokines by activating important intracellular signaling pathways during macrophage polarization [47]. Scavenging excessive RONS within macrophages is beneficial for promoting polarization towards M2 macrophages, thereby alleviating tissue inflammation [11, 48]. Therefore, the ability of C-NZ/GelMA hydrogels to scavenge intracellular RONS in macrophages was evaluated and further explored in terms of their impact on macrophage polarization and the inflammatory response.

First, the ability of C-NZ/GelMA to scavenge RONS from macrophages was qualitatively and quantitatively analyzed. The results showed a substantial reduction in

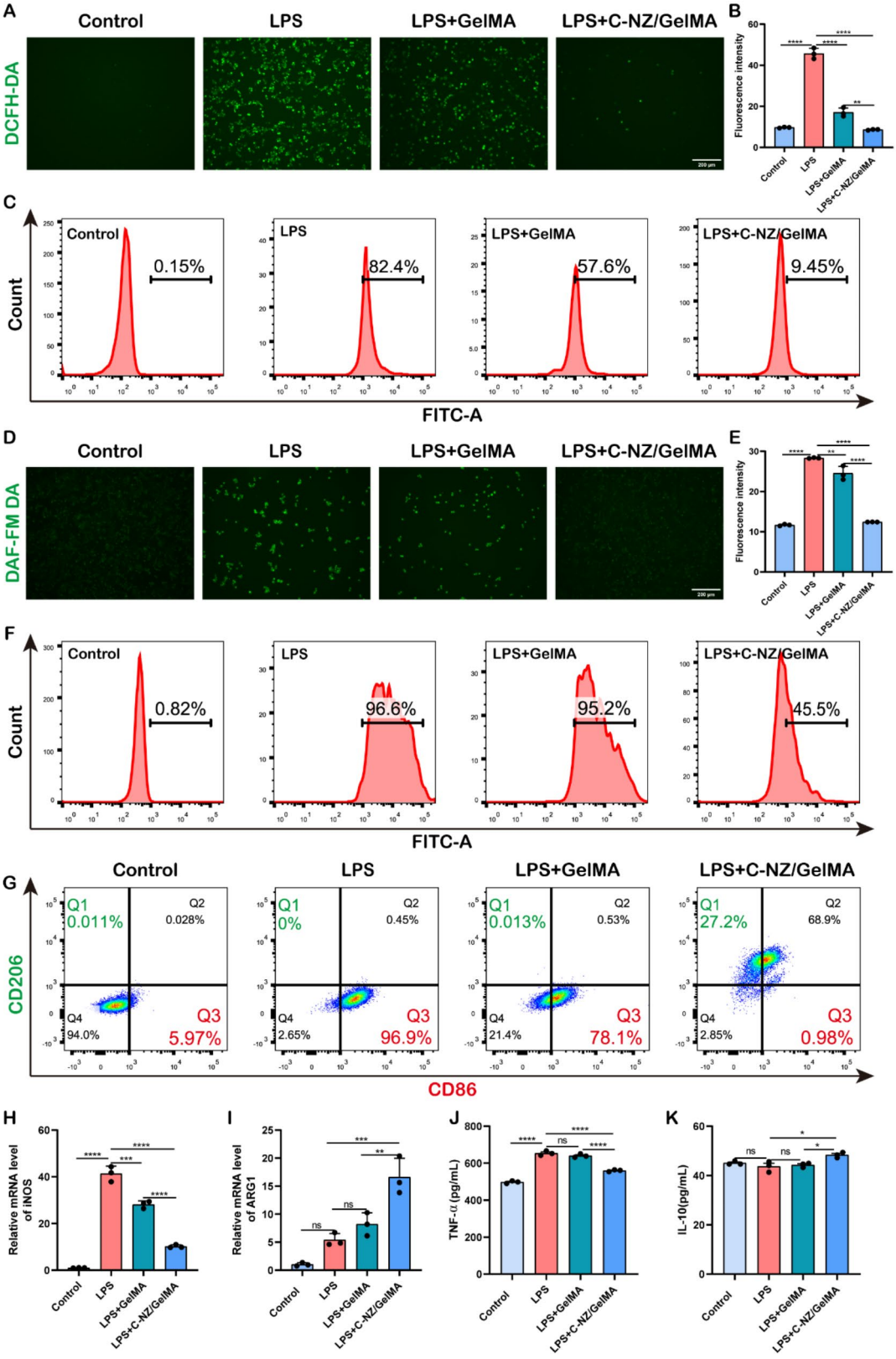

Fig. 4 (See legend on next page.)

(See figure on previous page.)

Fig. 4 Eliminated intracellular RONS and enhanced M2 polarization of RAW264.7 cells under LPS-induced oxidative stress conditions. **(A)** Fluorescence images of the total ROS observed in *Pg*-LPS treated RAW 264.7 cells using DCFH-DA probe and **(B)** quantitative fluorescence intensities **(C)** corresponding the total ROS level by FCM. Scale bar = 200 μm. **(D)** Fluorescence images of •NO level observed by the fluorescent probe DAF-FM DA and **(E)** quantitative fluorescence intensities **(F)** the corresponding quantitative result using FCM. Scale bar = 200 μm. **(G)** Representative FCM plots on the proportion of M1 phenotype (CD86) and M2 phenotype (CD206) macrophages. qPCR analysis results for the pro-inflammatory gene (iNOS) **(H)** and anti-inflammatory gene (ARG1) **(I)**. ELISA analysis results for TNF-α **(J)** and IL-10 **(K)**. Data are expressed as mean ± SD, $n = 3$. P-values are calculated using one-way ANOVA with Tukey's multiple comparisons test (ns, not significant; *$P<0.05$; **$P<0.01$; ***$P<0.001$ and ****$P<0.0001$)

green fluorescence in the C-NZ/GelMA group compared to the LPS group and GelMA group, approaching that of the control group (Fig. 4A and D). This finding was consistent with the results of the quantitative fluorescence intensity analysis (Fig. 4B and E). Further detection using FCM showed that after C-NZ/GelMA treatment, ROS intensity in RAW 264.7 cells decreased from 82.4 to 9.45%, and RNS intensity decreased from 96.6 to 45.5%. These results confirmed the effective scavenging of excessive RONS produced by *Pg*-LPS stimulation in RAW 264.7 cells by C-NZ/GelMA hydrogel (Fig. 4C and F).

To explore the effects of the materials on RAW 264.7 cell polarization, we assessed changes in the inflammatory response at both genetic and protein levels. FCM was employed to analyze the changes in the proportions of M1 macrophages (phenotypic marker CD86) and M2 macrophages (phenotypic marker CD206). Compared to those in the control group, the ratio of M1 macrophages in the LPS group significantly increased from 5.97 to 96.9%, while M2 macrophages were almost absent, indicating that *Pg*-LPS fully induced M1 macrophage polarization. Compared to those in the LPS group, the ratio of M1 macrophages in the GelMA group decreased from 96.9 to 78.1%, while the ratio of M2 macrophages remained very low (0.013%). In the C-NZ/GelMA group, the ratio of M1 macrophages significantly decreased from 96.9 to 0.98%, while M2 macrophages dramatically increased to 27.2% (Fig. 4G). These findings indicated that C-NZ/GelMA hydrogel could effectively reverse macrophage polarization from the M1 to M2 phenotype (Figure S10). In qPCR analysis, we examined the expression of the pro-inflammatory gene (iNOS) and the anti-inflammatory gene (ARG1). Due to the stimulation of *Pg*-LPS, iNOS gene expression was significantly higher in the LPS group and obviously decreased in the C-NZ/GelMA group (Fig. 4H). There was no significant difference in the expression of the anti-inflammatory gene ARG1 between the GelMA group and the LPS group, while the C-NZ/GelMA group exhibited a significant increase in ARG1 expression (Fig. 4I). ELISA assay kits were used to assess the levels of tumor necrosis factor-α (TNF-α) produced by M1 macrophages and interleukin-10 (IL-10) produced by M2 macrophages, which showed similar trends (Fig. 4J and K). In summary, C-NZ/GelMA exhibits a robust capability to promote the polarization of macrophages from the M1 to the M2 phenotype. This is reflected at both the genetic and protein levels.

ROS scavenging and anti-apoptosis effect of C-NZ/GelMA hydrogel in vivo

Considering the distinct physiological characteristics of upper incisors and molars in rats, we established a rat maxillary incisor and molar dental pulpitis model using *Pg*-LPS to comprehensively evaluate the therapeutic effects of C-NZ/GelMA [49, 50]. The procedure for dental pulpitis induction and treatment with the C-NZ/GelMA hydrogel is illustrated in Figs. 5A and 6A.

LPS-induced oxidative stress plays a crucial role in the pathological progression of dental pulpitis. Therefore, early inhibition of the accumulation of RONS is vital for alleviating dental pulp cell damage and necrosis [7]. Initially, we assessed oxidative stress indicators in dental pulp tissue. As shown in Fig. 5B, a substantial amount of NO was produced in dental pulp tissue two days after *Pg*-LPS exposure, where high NO levels induced nitrosative stress, leading to apoptosis, necrosis, and tissue damage [51]. After 3 days of C-NZ/GelMA hydrogel treatment, NO levels approached normal levels. The pulpitis+GelMA group did not show significant relief, remaining markedly higher than that of the control group even on the 7th day. H_2O_2, one of the most destructive radicals in the body, is often produced by macrophages in the fight against microbial invasion [52, 53]. Studies have demonstrated that H_2O_2 reduces pulp cell proliferation and differentiation, increases inflammation and apoptosis, and triggers cellular autophagy and premature senescence [54–56]. This study found that H_2O_2 content in dental pulpitis tissues significantly increased (Fig. 5C). Both experimental groups exhibited a noticeable decrease in H_2O_2 levels on the 3rd day. However, the pulpitis+C-NZ/GelMA group demonstrated a more reduction, maintaining a decreasing trend on the 7th day. Subsequently, we examined the changes in the expression of SOD and GPx (Fig. 5D and E). Insufficient antioxidants such as SOD and GPx can lead to dysregulation of dental pulpitis or an imbalance in redox reactions, resulting in excessive oxidative stress and inflammation [57]. Clearly, SOD and GPx activities in dental pulpitis tissues significantly decreased, consistent with the previously observed elevation in H_2O_2 and NO levels. Meanwhile, the SOD activity in C-NZ/GelMA-treated dental pulp tissue significantly recoverd on the 7th day of treatment.

Compared with that in the pulpitis group, GPx activity in the pulpitis+C-NZ/GelMA group also substantially increased on the third day.

To explore the anti-apoptotic effect of C-NZ/GelMA hydrogel, we employed TUNEL analysis to dynamically measure apoptotic cell alterations in dental pulp tissue (Figs. 5G and 6D, and S11). In the dental pulpitis group, a considerable amount of necrotic tissue was observed in the inflammatory cell infiltration area, with scattered apoptotic cells seen in the relatively healthy dental pulp tissue below the inflammatory area. On the 3rd day, necrotic areas in both treated groups were mainly concentrated in the inflammatory cell infiltration area, with an expanded area. On the 7th day, the pulpitis+C-NZ/GelMA group exhibited a significant reduction in necrotic apoptotic areas, even in the inflammatory cell infiltration area. Interestingly, on the 35th day, the pulpitis+C-NZ/GelMA group showed very few apoptotic cells in dental pulp tissue, almost indistinguishable from normal dental pulp tissue. In contrast, the pulpitis+GelMA group displayed a lot of apoptotic cells both near and away from the perforation site, potentially due to the lack of regulation in the oxidative stress environment, leading to continued tissue cell destruction by accumulated RONS.

These results confirm that C-NZ/GelMA hydrogel possesses significant antioxidant and RONS-scavenging capabilities. It regulates the excessive oxidative stress environment in dental pulpitis by scavenging RONS in vivo, thereby protecting dental pulp cells from apoptosis in dental pulpitis.

C-NZ/GelMA hydrogel enhances the polarization of macrophages toward the reparative M2 phenotype in vivo

To assess macrophage polarization, immunofluorescence staining and ELISA studies were conducted in vivo. Immunofluorescence images in Fig. 5H indicate a substantial presence of CD86-positive M1 macrophages (M1 macrophage surface marker) distributed around blood vessels and migrating from vessels to surrounding tissues in inflammatory pulp. This suggests that LPS-induced inflammatory response not only leads to proliferation of resident macrophages but also recruits new macrophages through the circulatory system to participate in the inflammatory reaction. On days 3 and 7 post-treatment with GelMA hydrogel, a significant number of CD86-positive M1 macrophages were still observed in dental pulp tissues. In contrast, the pulpitis+C-NZ/GelMA group had a considerable drop in the number of CD86-positive M1 macrophages starting from day 3 postoperatively, with almost no difference compared to the control group (Fig. 5H, S12, and 6E).

Subsequently, we observed changes in CD206-positive macrophages (M2 macrophage surface marker) in dental pulp tissues (Fig. 5I, S13, and 6F). In the dental pulpitis group, a substantial number of M2 macrophages were found to be mobilized and involved in the inflammatory response. In the pulpitis+GelMA group, we noticed a significant presence of CD206-positive M2 macrophages on days 3 and 7. In the molar model, a modest number of M2 macrophages were still present in the inflammation-infiltrated area on day 35. In the pulpitis+C-NZ/GelMA group, a dense population of CD206-positive macrophages was observed in dental pulp tissues on day 3, with an increasing number closer to the inflammation cell infiltration area. In comparison with the pulpitis+GelMA group, there was a notable downregulation of M2 macrophages on day 7. By day 35, the presence of M2 macrophages was almost non-observable. The results above indicate that C-NZ/GelMA hydrogel is extremely efficient in decreasing M1 macrophages, promoting macrophage polarization toward the M2 phenotype in the early stages of dental pulpitis, and accelerating the shift from the pro-inflammatory to the anti-inflammatory proliferative repair phase.

ELISA assays of pro-inflammatory cytokines TNF-α, IL-6, and anti-inflammatory cytokine IL-10 for rat maxillary incisor dental pulp tissues further corroborated the aforementioned observations (Fig. 5J and K, and Fig. 5L). The results indicated a significant upregulation of TNF-α, IL-6, and IL-10 in dental pulpitis tissues, suggesting that LPS-induced dental pulpitis fully mobilized the immune response. Starting from day 3, the pulpitis+C-NZ/GelMA group showed a rapid decrease in pro-inflammatory factors TNF-α and IL-6 levels compared to the dental pulpitis group, reaching normal levels. In the pulpitis+GelMA group, a noticeable decrease in TNF-α levels occurred only on day 7 compared to the dental pulpitis group, with no significant change in IL-6. IL-10 levels in pulp tissue were significantly higher in all experimental groups. However, the pulpitis+C-NZ/GelMA group exhibited the highest IL-10 content on day 3, decreasing by day 7. This pattern was consistent with the immunofluorescence results for CD86/CD206 in maxillary incisor dental pulp tissues.

C-NZ/GelMA hydrogel promotes pulp tissue regeneration and dentin repair in vivo

Histological analysis was utilized to assess the grades of inflammation and mineralization in pulp tissues and to observe the formation of reparative dentin, blood vessel formation, and pulp regeneration (Fig. 5F, Figure S14, and Fig. 6B). In the maxillary incisor dental pulpitis model, H&E staining revealed a tissue necrotic zone without cellular structure beneath the paper point two days after *Pg*-LPS stimulation. Adjacent to the necrotic zone was a densely populated area of inflammatory cell infiltration, localized within the dental pulp tissue near the injured

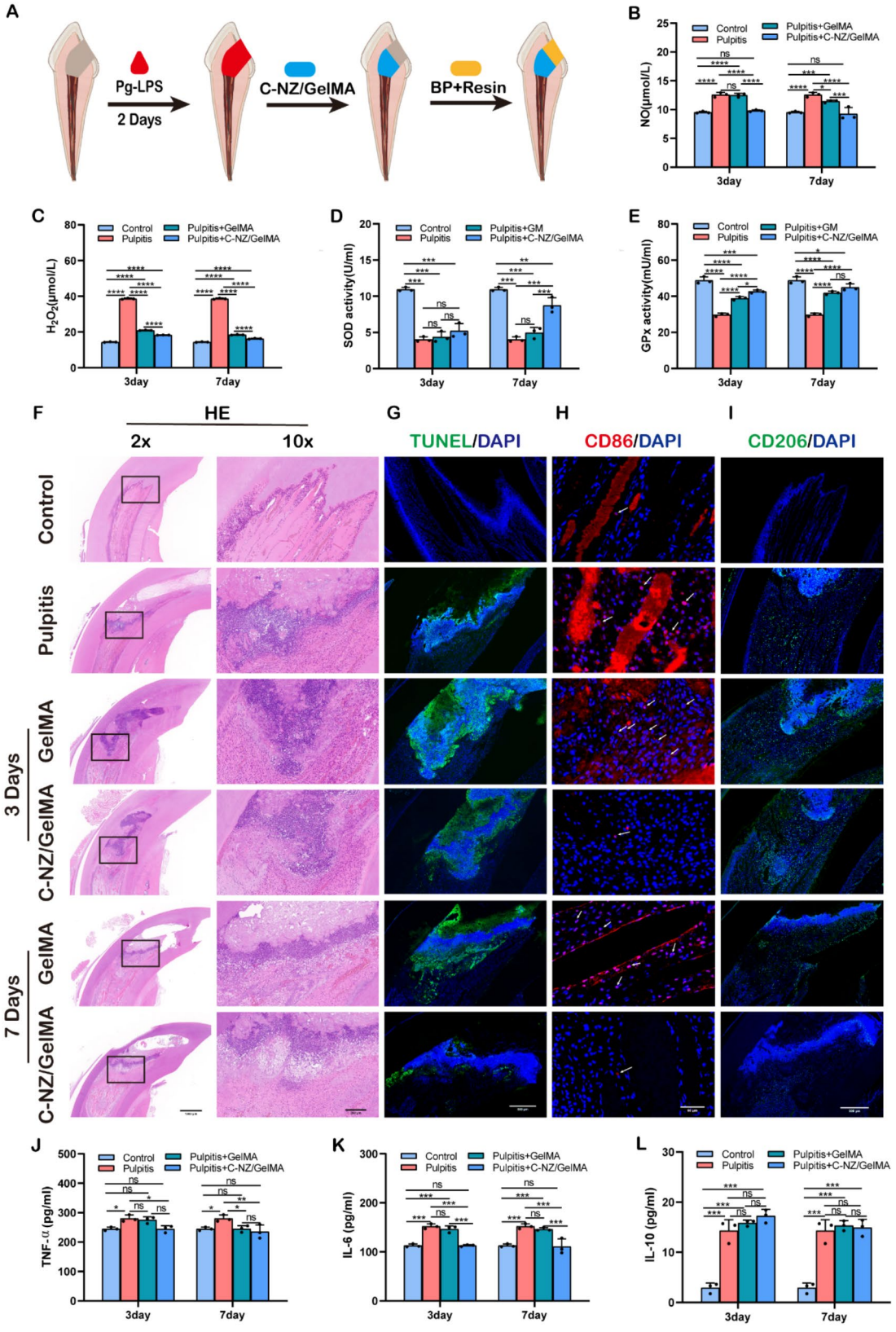

Fig. 5 (See legend on next page.)

(See figure on previous page.)

Fig. 5 Effect of C-NZ/GelMA hydrogel on oxidative stress and immune microenvironment in rat maxillary incisors. **(A)** Procedure for dental pulpitis induction and treatment with the C-NZ/GelMA hydrogel. **(B-E)** Oxidative stress indicators including NO, H_2O_2, SOD, and GPx in pulp tissue of rat pulpitis with treatment of GelMA or C-NZ/GelMA hydrogels. **(F)** H&E images showed the occurrence and development of rat pulpitis with treatment of GelMA or C-NZ/GelMA hydrogels. Right panels show magnified images of the box-enclosed area. Scale bars indicate 1000 μm (left figure) and 200 μm (right figure), respectively. **(G)** Representative immunofluorescence images of apoptotic population using TUNEL straining, scale bar = 500 μm. Immunofluorescence images of **(H)** CD86 and **(I)** CD206 in pulp tissue. Arrowheads indicate CD86-positive cells. Scale bars indicate 50 μm (CD86) and 500 μm (CD206), respectively. **(J-L)** ELISA analysis results for pro-inflammatory cytokines (TNF-α and IL-6) and anti-inflammatory cytokines (IL-10). Control: healthy pulp. Data are expressed as mean ± SD, $n = 3$. P-values are calculated using one-way ANOVA with Tukey's multiple comparisons test (ns, not significant; *$P<0.05$; **$P<0.01$; ***$P<0.001$ and ****$P<0.0001$)

site. After three days of gel treatment in both groups, an increased inflammatory infiltration area was observed, with the inflammatory infiltration area interspersed with the necrotic area. On day 7 post-treatment, the inflammatory area significantly decreased at the pulp-material interface in both treatment groups, with a more noticeable reduction in the tissue necrotic zone in the pulpitis + C-NZ/GelMA group. Interestingly, in the maxillary incisor dental pulp tissues of the pulpitis + C-NZ/GelMA group, a thick layer of cell-rich area with a uniform matrix structure and scattered small blood vessels appeared adjacent to the inflammatory infiltration area. This suggests that the dental pulpitis tissue has entered the repair-proliferative stage and that newly formed dental pulp tissue has gradually replaced the necrotic tissue (Fig. 5F). In the molar dental pulpitis model, H&E staining on days 3 and 7 also revealed similar inflammatory evolution processes (Figure S14).

On day 35, the pulpitis + C-NZ/GelMA group and pulpitis + GelMA group exhibited different outcomes in the treatment of rat molar dental pulpitis (Fig. 6B). H&E staining showed that in the region where the C-NZ/GelMA hydrogel was applied, it was replaced by regenerated pulp and reparative dentin. The reparative dentin closely adhered to the pulp walls, or surrounded dentin chips, with regularly arranged dentin tubules. A layer of odontoblast-like cells was neatly arranged beneath the reparative dentin, and no ectopic mineralized tissue was observed. Interestingly, newly formed dental pulp tissue with a lot of blood vessels appeared within the pulp chamber, indicating that C-NZ/GelMA promoted higher quality tissue regeneration in the dental pulpitis environment, not just a reparative response (Fig. 6B and Figure S15). In the pulpitis + GelMA group, the region where GelMA hydrogel was applied was filled with acellular necrotic tissue, and the dental pulp adjacent to the injury site was replaced by disordered calcified tissue and fibrous connective tissue lacking cellular structure. Inflammation cell infiltration was observed around the calcified tissue. Masson's trichrome staining further confirmed these results (Fig. 6C).

Treated teeth underwent micro-computed tomography (micro-CT) analysis to examine the formation of reparative dentin at the defect site (Figure S16 and Fig. 6G). The images showed preliminary dentin bridging in the pulpitis + C-NZ/GelMA group at day 7. By day 35, a well-defined, organized, and thick mineralized bridge was evident at the gel region's pulp-material interface, with a pulp space extending beneath the mineralized bridge in a regular and ordered manner. In the pulpitis + GelMA group, scattered mineralization was observed in the pulp chamber on day 7. By day 35, a thin layer of mineralized tissue was present in the hydrogel area, accompanied by ectopic mineralization within the pulp chamber. Quantitative analysis of the newly formed reparative dentin at day 35 indicated that the amount of reparative dentin formed in the pulpitis + GelMA group was less than that in the pulpitis + C-NZ/GelMA group (Fig. 6H).

The results of in vivo experiments demonstrate that the pulpitis + C-NZ/GelMA group can balance the oxidative stress microenvironment of pulpitis, alleviate pulp tissue damage, excellently regulate the immune environment to control inflammatory development, and promote tissue repair. This facilitates pulp regeneration and reparative dentin formation in pulpitis.

Conclusion

In summary, we developed an antioxidative system (C-NZ/GelMA) by combining antioxidase-mimicking C-NZ nanozymes with injectable and photocurable hydrogel as a pulp-capping material for VPT in dental pulpitis. The C-NZ/GelMA hydrogel has demonstrated excellent RONS-scavenging ability in both in vitro and in vivo experiments. It protects dental pulp cells from oxidative stress damage within the inflammatory microenvironment, promoting the polarization of macrophages from a pro-inflammatory M1 phenotype to a regenerative M2 phenotype. Additionally, the injectable C-NZ/GelMA hydrogel demonstrates excellent biocompatibility, suitable mechanical properties, degradation rates, and sustained release capabilities, meeting the main requirements for pulp-capping materials. Notably, rat dental pulpitis model reveals that direct pulp-capping treatment with C-NZ/GelMA hydrogel not only forms reparative dentin with regularly arranged dentinal tubules but also induces vascularized regeneration of dental pulp tissue. Our study confirms that C-NZ/GelMA hydrogel effectively promotes pulp regeneration in the inflammatory microenvironment, opening new horizons for bioactive materials in the treatment of pulpitis.

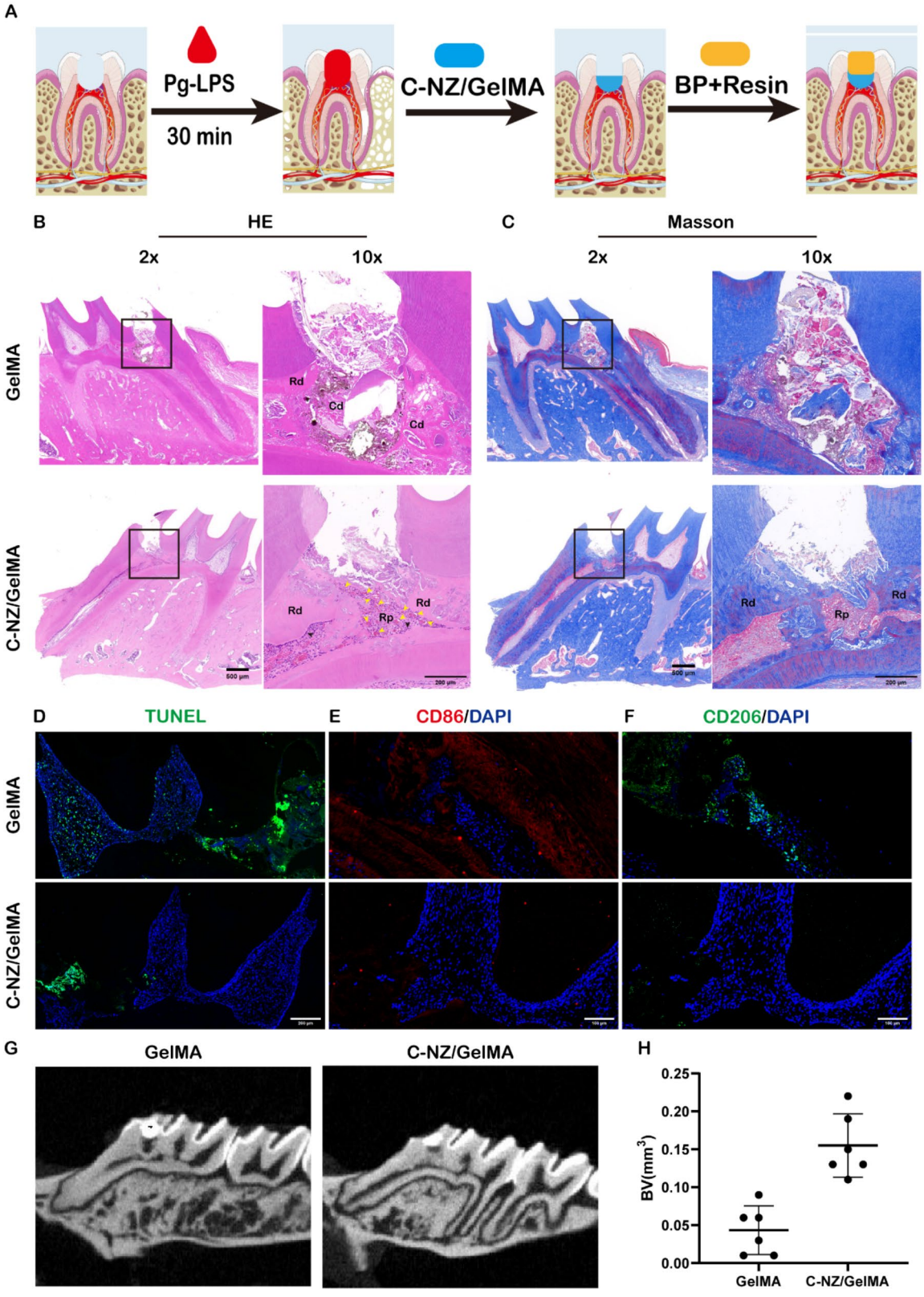

Fig. 6 (See legend on next page.)

(See figure on previous page.)

Fig. 6 Evaluation of C-NZ/GelMA hydrogel for pulp regeneration and dentin repair in a rat molar pulpitis model treated for 35 days. **(A)** Procedure for dental pulpitis induction and treatment with the C-NZ/GelMA hydrogel. **(B)** H&E images and **(C)** Masson's staining images showed the pulp regeneration and dentin repair of rat pulpitis with treatment of GelMA or C-NZ/GelMA hydrogels. Scale bars indicate 500 μm (left figure) and 200 μm (right figure), respectively. **(D)** Representative immunofluorescence images of apoptotic population using TUNEL straining, scale bar = 200 μm. **(E)** Immunofluorescence images of CD86 and **(F)** CD206 in pulp tissue, scale bar = 100 μm. **(G)** Micro-CT images showed the formation of reparative dentin at the defect site and **(H)** quantitative analysis of the reparative dentin volume. Rd: reparative dentin; Cd: cellular degeneration; Rp: regenerated pulp. Black arrows indicate odontoblast; yellow arrows indicate angiogenesis

Supplementary Information

The online version contains supplementary material available at https://doi.org/10.1186/s12951-024-02810-z.

Supplementary Material 1

Acknowledgements
The authors thank the supporting of the National Natural Science Foundation of China (No. 82160192), Key Project of the Joint Fund for Regional Innovation and Development of National Natural Science Foundation of China (U23A20686) and Research Fund of Guangxi Health Commission (Z20180682).

Author contributions
Yingjuan Zhang and Xianxian Huang: Conceptualization, Investigation, Methodology, Writing – Original Draft. Yicai Luo: Investigation. Xiangyu Ma: Investigation and Formal analysis. Ling Luo: Investigation. Ling Liang: Methodology. Tingting Deng: Investigation. Yang Qiao: Investigation. Fanggui Ye: Conceptualization, Methodology, Writing – Review & Editing. Hongbing Liao: Conceptualization, Funding Acquisition, Supervision, and Writing – Review & Editing.

Funding
This work was supported by the National Natural Science Foundation of China (No. 82160192), Key Project of the Joint Fund for Regional Innovation and Development of National Natural Science Foundation of China (U23A20686) and Research Fund of Guangxi Health Commission (Z20180682).

Data availability
The authors declare that the data supporting the findings of this study are available within the paper and its Supplementary Information files. Should any raw data files be needed in another format they are available from the corresponding author upon reasonable request.

Declarations

Ethics approval and consent to participate
The Guangxi Medical University Ethics Committee's guiding principles (Protocol Number: 202307004, 202307435 and 2023015) were followed in all experiments.

Consent for publication
All authors consent for publication.

Competing interests
The authors declare no competing interests.

Received: 6 June 2024 / Accepted: 23 August 2024
Published online: 04 September 2024

References

1. Duncan HF, Kirkevang LL, Peters OA, El-Karim I, Krastl G, Del Fabbro M, Chong BS, Galler KM, Segura-Egea JJ, Kebschull M, Participants ESEW, Methodological C. Treatment of pulpal and apical disease: the European Society of Endodontology (ESE) S3-level clinical practice guideline. Int Endod J. 2023;56(Suppl 3):238–95.
2. AAE Position Statement on Vital Pulp Therapy. J Endod. 2021;47(9):1340–4.
3. Islam R, Islam MRR, Tanaka T, Alam MK, Ahmed HMA, Sano H. Direct pulp capping procedures - evidence and practice. Jpn Dent Sci Rev. 2023;59:48–61.
4. Bossu M, Mancini P, Bruni E, Uccelletti D, Preziosi A, Rulli M, Relucenti M, Donfrancesco O, Iaculli F, Di Giorgio G, Matassa R, Salucci A, Polimeni A. Biocompatibility and Antibiofilm properties of Calcium Silicate-based cements: an in vitro evaluation and report of two clinical cases. Biology (Basel) 10(6) (2021).
5. Duncan HF, Smith AJ, Fleming GJ, Cooper PR. HDACi: cellular effects, opportunities for restorative dentistry. J Dent Res. 2011;90(12):1377–88.
6. Duncan HF, Kobayashi Y, Kearney M, Shimizu E. Epigenetic therapeutics in dental pulp treatment: hopes, challenges and concerns for the development of next-generation biomaterials. Bioact Mater. 2023;27:574–93.
7. Dogan Buzoglu H, Ozcan M, Bozdemir O, Aydin Akkurt KS, Zeybek ND, Bayazit Y. Evaluation of oxidative stress cycle in healthy and inflamed dental pulp tissue: a laboratory investigation. Clin Oral Investig. 2023;27(10):5913–23.
8. Korkmaz Y, Plomann M, Puladi B, Demirbas A, Bloch W, Deschner J. Dental Pulp inflammation initiates the occurrence of mast cells expressing the alpha(1) and beta(1) subunits of Soluble Guanylyl Cyclase. Int J Mol Sci 24(2) (2023).
9. Forman HJ, Zhang H. Targeting oxidative stress in disease: promise and limitations of antioxidant therapy. Nat Rev Drug Discov. 2021;20(9):689–709.
10. Zaky SH, Shehabeldin M, Ray H, Sfeir C. The role of inflammation modulation in dental pulp regeneration. Eur Cells Mater. 2021;41:184–93.
11. Tsai CF, Chen GW, Chen YC, Shen CK, Lu DY, Yang LY, Chen JH, Yeh WL. Regulatory effects of Quercetin on M1/M2 macrophage polarization and Oxidative/Antioxidative balance. Nutrients 14(1) (2021).
12. Lee YH, Kim GE, Song YB, Paudel U, Lee NH, Yun BS, Yu MK, Yi HK. Davallialactone reduces inflammation and repairs dentinogenesis on glucose oxidase-induced stress in dental pulp cells. J Endod. 2013;39(11):1401–6.
13. Baumgardner KR, Sulfaro MA. The anti-inflammatory effects of human recombinant copper-zinc superoxide dismutase on pulp inflammation. J Endod. 2001;27(3):190–5.
14. Pan Z, Dong H, Huang N, Fang J. Oxidative stress and inflammation regulation of sirtuins: new insights into common oral diseases. Front Physiol. 2022;13:953078.
15. Guo X, Chen J. The protective effects of saxagliptin against lipopolysaccharide (LPS)-induced inflammation and damage in human dental pulp cells. Artif Cells Nanomed Biotechnol. 2019;47(1):1288–94.
16. Liang C, Wu W, He X, Xue F, Feng D. Circ_0138960 knockdown alleviates lipopolysaccharide-induced inflammatory response and injury in human dental pulp cells by targeting miR-545-5p/MYD88 axis in pulpitis. J Dent Sci. 2023;18(1):191–202.
17. Zhang P, Cui Z, Li S. The protective effects of S14G-humanin (HNG) against lipopolysaccharide (LPS)- induced inflammatory response in human dental pulp cells (hDPCs) mediated by the TLR4/MyD88/NF-κB pathway. Bioengineered. 2021;12(1):7552–62.
18. Wang H, Chen X, Zhang L, Han Z, Zheng J, Qi Y, Zhao W, Xu X, Li T, Zhou Y, Bao P, Xue X. Dual-fuel propelled nanomotors with two-stage permeation for deep bacterial infection in the treatment of Pulpitis. Adv Sci (Weinh). 2024;11(5):e2305063.
19. Luo N, Deng YW, Wen J, Xu XC, Jiang RX, Zhan JY, Zhang Y, Lu BQ, Chen F, Chen X. Wnt3a-Loaded hydroxyapatite Nanowire@Mesoporous silica core-Shell Nanocomposite promotes the regeneration of dentin-pulp Complex via Angiogenesis, oxidative stress resistance, and odontogenic induction of stem cells. Adv Healthc Mater. 2023;12(22):e2300229.
20. Huang Y, Ren J, Qu X. Nanozymes: classification, Catalytic mechanisms, Activity Regulation, and applications. Chem Rev. 2019;119(6):4357–412.
21. Ren X, Chen D, Wang Y, Li H, Zhang Y, Chen H, Li X, Huo M. Nanozymes-recent development and biomedical applications. J Nanobiotechnol. 2022;20(1):92.
22. Rizwana N, Agarwal V, Nune M. Antioxidant for neurological diseases and Neurotrauma and Bioengineering approaches. Antioxidants 11(1) (2021).
23. Shang L, Yu Y, Jiang Y, Liu X, Sui N, Yang D, Zhu Z. Ultrasound-augmented multienzyme-like Nanozyme Hydrogel Spray for promoting Diabetic Wound Healing. ACS Nano. 2023;17(16):15962–77.

24. Xiang J, Yang X, Tan M, Guo J, Ye Y, Deng J, Huang Z, Wang H, Su W, Cheng J, Zheng L, Liu S, Zhong J, Zhao J. NIR-enhanced pt single atom/g-C3N4 nanozymes as SOD/CAT mimics to rescue ATP energy crisis by regulating oxidative phosphorylation pathway for delaying osteoarthritis progression. Bioactive Mater. 2024;36:1–13.
25. Feng Y, Luo X, Li Z, Fan X, Wang Y, He RR, Liu M. A ferroptosis-targeting ceria anchored halloysite as orally drug delivery system for radiation colitis therapy. Nat Commun. 2023;14(1):5083.
26. Xu YY, Luo YF, Weng ZZ, Xu HC, Zhang W, Li Q, Liu HJ, Liu LB, Wang YM, Liu XX, Liao L, Wang XL. Microenvironment-responsive metal-phenolic nanozyme release platform with Antibacterial, ROS Scavenging, and Osteogenesis for Periodontitis. ACS Nano. 2023;17(19):18732–46.
27. Xie F, Zhu C, Gong L, Zhu N, Ma Q, Yang Y, Zhao X, Qin M, Lin Z, Wang Y. Engineering core-shell chromium nanozymes with inflammation-suppressing, ROS-scavenging and antibacterial properties for pulpitis treatment. Nanoscale. 2023;15(34):13971–86.
28. Mu X, Wang J, He H, Li Q, Yang B, Wang J, Liu H, Gao Y, Ouyang L, Sun S, Ren Q, Shi X, Hao W, Fei Q, Yang J, Li L, Vest R, Wyss-Coray T, Luo J, Zhang XD. An oligomeric semiconducting nanozyme with ultrafast electron transfers alleviates acute brain injury. Sci Adv. 2021;7(46):eabk1210.
29. Guo X, Li J, Wu Y, Xu L. Recent advancements in hydrogels as novel tissue engineering scaffolds for dental pulp regeneration. Int J Biol Macromol 264 (2024).
30. Kurian AG, Singh RK, Patel KD, Lee JH, Kim HW. Multifunctional GelMA platforms with nanomaterials for advanced tissue therapeutics. Bioact Mater. 2022;8:267–95.
31. Qian Y, Gong J, Lu K, Hong Y, Zhu Z, Zhang J, Zou Y, Zhou F, Zhang C, Zhou S, Gu T, Sun M, Wang S, He J, Li Y, Lin J, Yuan Y, Ouyang H, Yu M, Wang H. DLP printed hDPSC-loaded GelMA microsphere regenerates dental pulp and repairs spinal cord. Biomaterials. 2023;299:122137.
32. Wu Y, Li X, Sun Y, Tan X, Wang C, Wang Z, Ye L. Multiscale design of stiffening and ROS scavenging hydrogels for the augmentation of mandibular bone regeneration. Bioact Mater. 2023;20:111–25.
33. Luo L, He Y, Jin L, Zhang Y, Guastaldi FP, Albashari AA, Hu F, Wang X, Wang L, Xiao J, Li L, Wang J, Higuchi A, Ye Q. Application of bioactive hydrogels combined with dental pulp stem cells for the repair of large gap peripheral nerve injuries. Bioact Mater. 2021;6(3):638–54.
34. Xia C, Zhu S, Feng T, Yang M, Yang B. Evolution and synthesis of Carbon dots: from Carbon dots to Carbonized Polymer dots. Adv Sci (Weinh). 2019;6(23):1901316.
35. Yang L, Dong S, Gai S, Yang D, Ding H, Feng L, Yang G, Rehman Z, Yang P. Deep insight of design, mechanism, and Cancer Theranostic Strategy of Nanozymes. Nanomicro Lett. 2023;16(1):28.
36. Kedare SB, Singh RP. Genesis and development of DPPH method of antioxidant assay. J Food Sci Technol. 2011;48(4):412–22.
37. Ozcan B, Bayrak E, Erisken C. Characterization of Human Dental Pulp tissue under Oscillatory Shear and Compression. J Biomech Eng. 2016;138(6):061006.
38. Liu C, Yu Q, Yuan Z, Guo Q, Liao X, Han F, Feng T, Liu G, Zhao R, Zhu Z, Mao H, Zhu C, Li B. Engineering the viscoelasticity of gelatin methacryloyl (GelMA) hydrogels via small dynamic bridges to regulate BMSC behaviors for osteochondral regeneration. Bioact Mater. 2023;25:445–59.
39. Kurian AG, Mandakhbayar N, Singh RK, Lee JH, Jin G, Kim HW. Multifunctional dendrimer@nanoceria engineered GelMA hydrogel accelerates bone regeneration through orchestrated cellular responses. Mater Today Bio. 2023;20:100664.
40. Zhang Y, Chen H, Li J. Recent advances on gelatin methacrylate hydrogels with controlled microstructures for tissue engineering. Int J Biol Macromol. 2022;221:91–107.
41. Wang Y, Lv T, Yin K, Feng N, Sun X, Zhou J, Li H. Carbon dot-based hydrogels: preparations, properties, and applications, small. (Weinheim Der Bergstrasse Germany). 2023;19(17):e2207048.
42. He J, Sun Y, Gao Q, He C, Yao K, Wang T, Xie M, Yu K, Nie J, Chen Y, He Y. Gelatin methacryloyl hydrogel, from standardization, performance, to Biomedical Application. Adv Healthc Mater. 2023;12(23):e2300395.
43. Huang M, Zhan C, Yang X, Hou J. Regulated cell death in Pulpitis. J Endod. 2020;46(10):1403–13.
44. Sun Y, Sun X, Li X, Li W, Li C, Zhou Y, Wang L, Dong B. A versatile nanocomposite based on nanoceria for antibacterial enhancement and protection from aPDT-aggravated inflammation via modulation of macrophage polarization. Biomaterials. 2021;268:120614.
45. Weissman D, Maack C. Mitochondrial function in macrophages controls cardiac repair after myocardial infarction. J Clin Invest 133(4) (2023).
46. Yang Y, Guo L, Wang Z, Liu P, Liu X, Ding J, Zhou W. Targeted silver nanoparticles for rheumatoid arthritis therapy via macrophage apoptosis and re-polarization. Biomaterials. 2021;264:120390.
47. Rendra E, Riabov V, Mossel DM, Sevastyanova T, Harmsen MC, Kzhyshkowska J. Reactive oxygen species (ROS) in macrophage activation and function in diabetes. Immunobiology. 2019;224(2):242–53.
48. Zhang B, Yang Y, Yi J, Zhao Z, Ye R. Hyperglycemia modulates M1/M2 macrophage polarization via reactive oxygen species overproduction in ligature-induced periodontitis. J Periodontal Res. 2021;56(5):991–1005.
49. Song T, Li X, Liu L, Zeng Y, Song D, Huang D. The effect of BMP9 on inflammation in the early stage of pulpitis. J Appl Oral Sci. 2023;31:e20220313.
50. Liu X, Wang C, Pang L, Pan L, Zhang Q. Combination of resolvin E1 and lipoxin A4 promotes the resolution of pulpitis by inhibiting NF-kappaB activation through upregulating sirtuin 7 in dental pulp fibroblasts. Cell Prolif. 2022;55(5):e13227.
51. Zhao C, Chen J, Zhong R, Chen DS, Shi J, Song J. Oxidative-species-selective materials for diagnostic and therapeutic applications. Angew Chem Int Ed Engl. 2021;60(18):9804–27.
52. Lobo V, Patil A, Phatak A, Chandra N. Free radicals, antioxidants and functional foods: impact on human health. Pharmacogn Rev. 2010;4(8):118–26.
53. Żukowski P, Maciejczyk M, Waszkiel D. Sources of free radicals and oxidative stress in the oral cavity. Arch Oral Biol. 2018;92:8–17.
54. Vaseenon S, Srisuwan T, Chattipakorn N, Chattipakorn SC. Lipopolysaccharides and hydrogen peroxide induce contrasting pathological conditions in dental pulpal cells. Int Endod J. 2023;56(2):179–92.
55. Prakash R, Fauzia E, Siddiqui AJ, Yadav SK, Kumari N, Shams MT, Naeem A, Praharaj PP, Khan MA, Bhutia SK, Janowski M, Boltze J, Raza SS. Oxidative stress-induced autophagy compromises stem cell viability, stem cells (Dayton. Ohio). 2022;40(5):468–78.
56. Ok CY, Park S, Jang HO, Takata T, Lee OH, Bae MK, Bae SK. FK866 protects human Dental Pulp cells against oxidative stress-Induced Cellular Senescence, antioxidants (Basel. Switzerland) 10(2) (2021).
57. Yang X, Xiang J, Su W, Guo J, Deng J, Tang L, Li G, Liang Y, Zheng L, He M, Zhong J, Zhao J. Modulating pt nanozyme by using isolated cobalt atoms to enhance catalytic activity for alleviating osteoarthritis. Nano Today 49 (2023).

Publisher's note